Soft Matter

ROYAL SOCIETY OF CHEMISTRY

PAPER

View Article Online
View Journal | View Issue



Cite this: *Soft Matter*, 2020, **16**, 2321

# An eco-friendly pathway to thermosensitive micellar nanoobjects *via* photoRAFT PISA: the full guide to poly(*N*-acryloylpyrrolidin)-*block*-polystyrene diblock copolymers†

Felix Lauterbach and Volker Abetz *

Received 18th December 2019,
Accepted 17th January 2020

DOI: 10.1039/c9sm02483b

rsc.li/soft-matter-journal

Spherical macromolecular assemblies, so-called latexes, consisting of polystyrene (PS) resemble a relevant class of synthetic polymers used for a plethora of applications ranging from coatings or lubricants to biomedical applications. Their synthesis is usually tailored to the respective application where emulsifiers, radical initiators, or other additives still play a major role in achieving the desired properties. Herein, we demonstrate an alternative based on the photoiniferter reversible addition–fragmentation chain transfer (RAFT) polymerization-induced self-assembly (PISA) of Poly(*N*-acryloylpyrrolidin)-*block*-polystyrene (PAPy-*b*-PS). This approach yields monodisperse nanospheres with tunable sizes based on an aqueous formulation with only two ingredients. These nanospheres are additionally thermosensitive, meaning that they change their hydrodynamic diameter linearly with the temperature in a broad range between 10 °C and 70 °C. Combined with the eco-friendly synthesis in pure water at 40 °C, the herein presented route constitutes an unprecedented pathway to thermosensitive diblock copolymer aggregates in short reaction times without any additives.



## 1 Introduction

The emulsion polymerization of styrene has historically been one of the most studied heterogeneous systems in polymer chemistry; first formulations were already invented in 1942 and played a significant role in understanding the mechanism of emulsion polymerization.[1,2] Since then, waterborne polystyrene latexes have been widely used in academia for purposes like size calibration (*e.g.* in electron microscopy, cell counters,[3] agarose gel electrophoresis,[4] *etc.*), agglutination tests,[5,6] and phagocytosis experiments,[7] as well as in industrial branches that deal with *e.g.* pigments,[8] adhesives,[9] or other coatings.[10] For a long time, those latexes were made by free radical emulsion polymerization using surfactants as emulsifiers to control their size and surface activity.

With the invention of controlled radical polymerization (CRP) mechanisms based on the reversible deactivation radical polymerization (RDRP) and their ability to produce block copolymers in a straightforward way, the use of surfactants became redundant as the required (macromolecular) chain transfer agent (CTA) could be used for both deactivating the growing polymer chains and stabilizing them in the surrounding aqueous medium.[11–13] Further advantages of combining CRP techniques with emulsion polymerization to produce industrially relevant (block)copolymers are obvious: Waterborne processes are not only cheap, they moreover provide efficient heat transfer, a low viscosity, and renounce volatile organic compounds, while coincidently giving rise to well-defined polymer architectures.[14–16]

Several methods based on the RDRP mechanism have been developed, the most common ones being the atom transfer radical polymerization (ATRP),[17,18] nitroxide-mediated polymerization (NMP),[19] and RAFT polymerization.[20,21] Besides the conventional thermal initiation, these methods allow control through external physical (light irradiation, ultrasonication)[22–25] and chemical stimuli (metal-, redox-, enzyme-, Lewis acid-, or electrochemically-catalyzed),[26–30] with light being lately one of the most prominent initiation sources.[31] Using light as an external source allows highly resolved spatiotemporal control while making an adjustment of the radical concentration independent of the reaction temperature. By decoupling the concentration of active species from temperature, the use of thermoresponsive stabilizing blocks in polymerization-induced self-assembly (PISA) becomes further convenient. It is no longer required to make complex, hydrophilic stabilizers consisting of two or more monomer species,[32,33] as one can simply tune the temperature so that the thermoresponsive polymer is still soluble. In the case of polymers with a lower critical solution temperature (LCST) the working temperature can

*Institute of Physical Chemistry, Universität Hamburg, Grindelallee 117, 20146 Hamburg, Germany. E-mail: volker.abetzt@chemie.uni-hamburg.de*

† Electronic supplementary information (ESI) available. See DOI: 10.1039/c9sm02483b

be kept below the LCST so that the polymer does not collapse. It is worth noting that the rate of polymerization still depends on the thermal energy introduced to overcome the activation energy, however, deploying the advantages of light initiation makes PISA a more straightforward, universally applicable, and therefore industrially interesting process. Moreover, precise tailoring of the aggregate sizes and properties is of high interest, both from a fundamental and application point of view.

In here we present an unelaborate and cost-effective route to thermoresponsive diblock copolymer aggregates in aqueous solution *via* a two-step synthetic procedure (Fig. 1). The water-soluble PAPy block is polymerized *via* RAFT in the first step at 70 °C in a mixture of water and 1,4-dioxane in a continuous flow microreactor (see Fig. S1, ESI†). This is followed by an *ab initio* emulsion polymerization of styrene in batch conducted at 40 °C (see Fig. S2, ESI†) exhibiting particularly fast reaction kinetics – at such a low temperature – so that almost quantitative monomer conversions can be reached within less than five to eight hours. Additionally, three different trithiocarbonates (TTC) as CTA are studied to investigate the effect of endgroup functionality on the particle size distribution (PSD), stability of the emulsion, and reaction rate. The final diblock copolymer aggregates are furthermore studied regarding their thermosensitive behavior in solution *via* extensive dynamic light scattering (DLS) to proof the tunability of the aggregate size over a broad range of temperatures.

## 2 Results and discussion

### 2.1 Homopolymerization of *N*-acryloylpyrrolidine

PAPy homopolymers and copolymers containing APy have been extensively investigated by our group in preceding studies.[33–35] They have proven to exhibit a peculiar thermoresponsive behavior in aqueous solutions with an LCST of the homopolymer around 50 °C. For this study, five different PAPy homopolymers with phase transition temperatures (PTT) between 42 °C and 50 °C have been prepared that vary in molecular weight as well as endgroups with the scope to uncover the most feasible and universally applicable formulation for the subsequent PISA with styrene. The respective polymers as well as analytical data are depicted in Table 1.

Table 1 Comparison of all synthesized PAPy homopolymers with assignment of their endgroup according to the used CTA, number-averaged theoretical weight calculated from monomer conversion (the measured $M_n$ can be found in Table S1, ESI), the average number of APy repeating units, as well as dispersity, and PTT in water taken from visual turbidimetry. The solution pH in water was purposely not adjusted with additives so that it stayed always at around 5 for the homopolymers with $TTC_1$ and $TTC_2$ endgroups and at around 7 for the homopolymer with the $TTC_3$ endgroup, respectively

| Sample code | End group[a] | $\bar{M}_{n,theor.}$[b]/kDa | $N_{rep.\,units}$[b] | $Đ$[c] | PTT[d]/°C |
|---|---|---|---|---|---|
| $PAPy^{13.8}$-$TTC_1$ | $TTC_1$ | 14.1 | 110 | 1.36 | 50.2 |
| $PAPy^{3.1}$-$TTC_2$ | $TTC_2$ | 3.5 | 25 | 1.39 | 41.6 |
| $PAPy^{8.2}$-$TTC_2$ | $TTC_2$ | 8.6 | 66 | 1.33 | 47.0 |
| $PAPy^{23.6}$-$TTC_2$ | $TTC_2$ | 23.9 | 188 | 1.51 | 46.5 |
| $PAPy^{9.7}$-$TTC_3$ | $TTC_3$ | 10.0 | 77 | 1.29 | 47.1 |

[a] See Fig. 1. [b] Number averaged molecular weight and degree of polymerization calculated from monomer conversion which is given by $^1$H-NMR measurements (see ESI, eqn (S1) and (S3)). [c] Dispersity index determined by SEC in DMAc at 50 °C. [d] Phase transition temperature determined by visual turbidimetry in water at a concentration of 1% (w/w).

It becomes evident that the PAPy homopolymer which contains a butyl endgroup on one side of the polymer chain and a carboxylic acid (which is partially deprotonated at the resulting pH of 5) on the other ($PAPy^{13.8}$-$TTC_1$) shows the highest PTT. These functionalities make the whole polymer slightly more hydrophilic compared to PAPy homopolymers with similar chain length but a longer alkyl chain as an endgroup (compare $PAPy^{8.2}$-$TTC_2$). Consequently, the homopolymer with the shortest hydrophilic block and a dodecyl endgroup exhibits the lowest PTT. Surprisingly, exchanging the carboxylic acid on the α-terminal end with a non-ionizable residue does not significantly influence the solubility behavior (compare $PAPy^{8.2}$-$TTC_2$ and $PAPy^{9.7}$-$TTC_3$). The determination of the PTT by the onset of the clouding in visual turbidimetry, however, is sometimes operator-dependent and hence only indicative of the actual phase transition.[36] Thus, we performed temperature-resolved DLS measurements of the PAPy homopolymers at the same concentration (1% (w/w)) in aqueous solution.

The resulting intensity correlation functions were fitted with the cumulant approach (see eqn (S4), ESI†) and evaluated *via* the Stokes–Einstein relation (eqn (S5), ESI†). They revealed

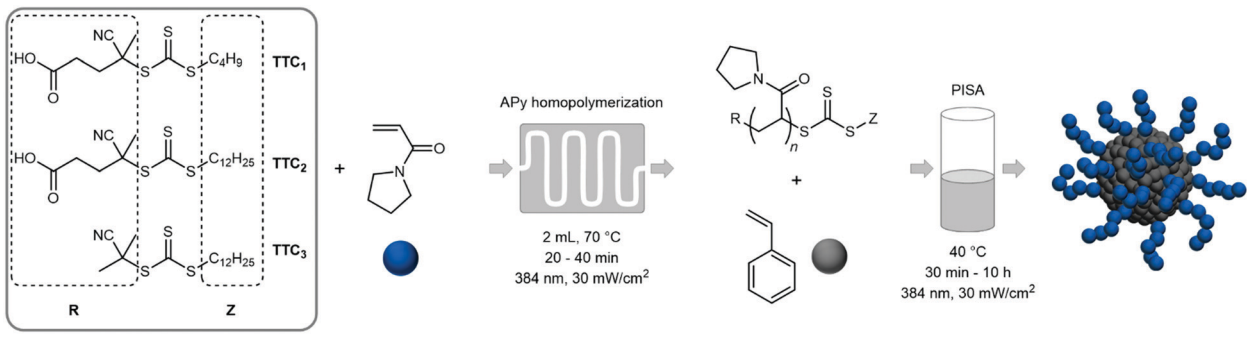


Fig. 1 Two-step solution–emulsion photoiniferter RAFT polymerization of *N*-acryloylpoyrrolidin (APy) and styrene with various RAFT agents. APy is polymerized first in a continuous flow setup followed by the *ab initio* emulsion polymerization of styrene in water.

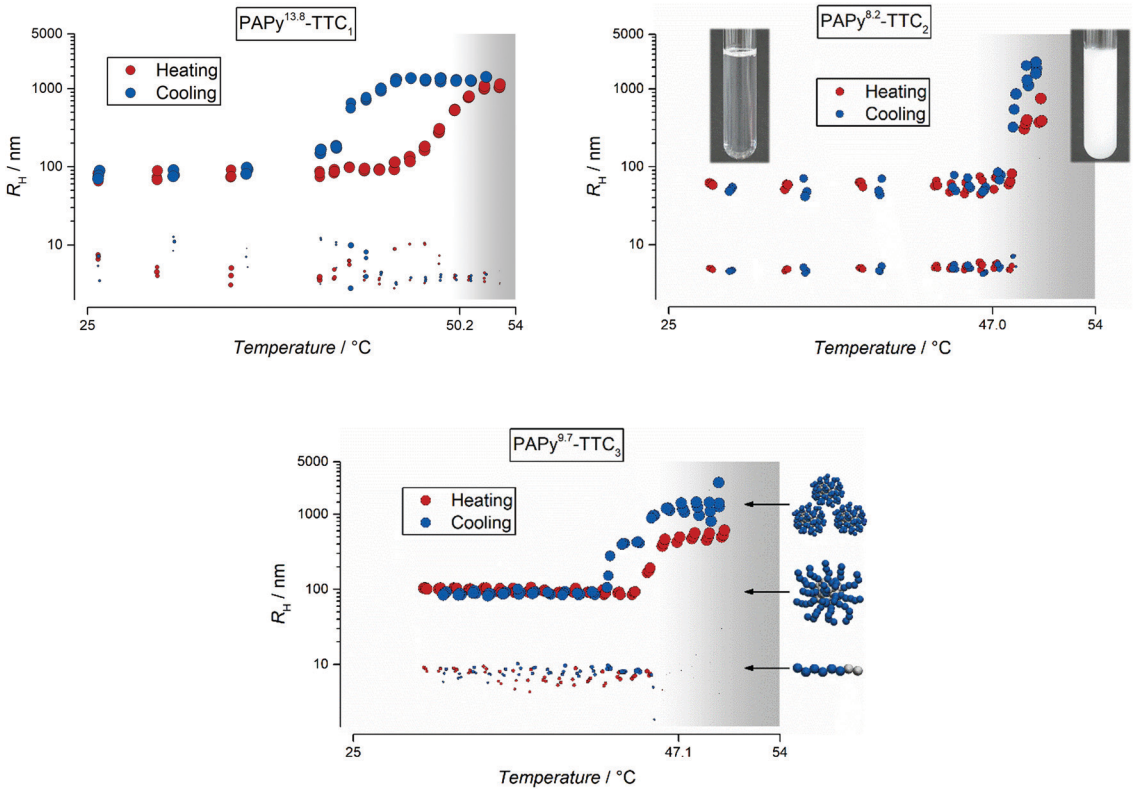


Fig. 2 Temperature-dependent evolution of the hydrodynamic radii from three relevant PAPy homopolymers with different lengths and endgroups in aqueous solution ($c$ = 1% (w/w)) obtained by DLS. The red dots depict the radii during heating of the polymer solution while the blue dots represent the respective radii during the cooling step. In all homopolymer samples the most suitable fit indicated two distinct aggregate species; both are shown in the graphs with different marker sizes, while the area of the marker represents the relative scattering intensity of the particular species. The optical cloud point observed *via* turbidimetry is indicated as the background (transition from white to grey).

some distinctive and peculiar thermoresponsive properties of the homopolymer and its aggregates in water as depicted in Fig. 2.

From the cumulant (Fig. 2) and more elaborate CONTIN analysis (see Fig. S12, S14, and S15, ESI†) it becomes obvious that the temperature-dependent and reversible aggregation of the PAPy homopolymers is by far more complex than usually assumed by just looking at the often deceptive courses of the scattering intensity with temperature (exemplarily shown in Fig. S15, ESI†). The scattering intensity is often considered solely for the investigation of an LCST behavior.[37–39] However, we can show that fitting the intensity correlation function obtained from the DLS measurement with multiple exponential decays often yields deeper insights into the complex aggregation that takes places at the transition from a mostly dissolved to an agglomerated state.

For all the homopolymer samples investigated in this study we found that already at temperatures below the LCST there are two different species present in aqueous solution. One species corresponds to well-dissolved unimers with hydrodynamic radii of typically below 10 nm; the other species consists of polymeric aggregates – potentially micelles – due to the already slightly amphiphilic character of the homopolymer. This may sound reasonable for the polymers with a dodecyl endgroup, yet unintuitive for the PAPy$^{13.8}$-TTC$_1$ that only has a butyl residue at the ω-terminal end. The shorter alkyl chain as the hydrophobic endgroup, thus, could be the reason for the slightly more pronounced hysteresis compared to the polymers with longer alkyl chains: reorganization from a higher agglomeration level needs probably more time when the amphiphilic character is less pronounced. This might be attributed to differently structured particles above the LCST – while more amphiphilic polymers could form micelles, less amphiphilic polymers probably build up more entanglements first which efficiently hampers dissolution upon cooling.

It becomes furthermore apparent that although the carboxylic acid at the α-terminal end does not significantly affect the position of the PPT, it nonetheless seems to influence the aggregation behavior at the PTT. Upon heating of the polymer solution, the pre-formed macromolecular aggregates agglomerate and grow further, additionally catching the unimers which are almost completely absent above the phase transition. During the cooling step – but still above the LCST – these aggregates that at this point have grown to the micrometer size still agglomerate further. Interestingly, no precipitates formed although the polymer–water system had enough time above the LCST to undergo macrophase separation. It indicates that there is still enough stabilization of the admittedly big aggregates by some soluble hydrophilic side groups of the PAPy homopolymer. Below the phase transition of PAPy$^{9.7}$-TTC$_3$, instead

of smoothly and progressively disassembling into the stable aggregates as in the case of $PAPy^{8.2}$-$TTC_2$, this polymer shows a two-step aggregation that is distinctly visible upon cooling of the sample. This behavior is reproducible during three heating–cooling cycles with slow heating/cooling rates (compare Fig. S16, ESI†) proving that this is not a kinetic effect but rather a thermodynamically stable feature of the aggregation behavior. The three different sketches in Fig. 2 (unimers, micelles, and accumulated micelles) represent the three different species present in the temperature-dependent DLS measurements. Those species have been described for a different polymer in excellent detail by Eggers *et al.* and explanations especially for coil-to-globule transitions can be found there.[40]

That this two-step aggregation is not observable for the homopolymer with the carboxylic acid endgroup ($TTC_2$-end-capped), might be attributed to the more hydrophilic corona of the pre-formed particle. Carboxylic acid functionalities could favor the almost instantaneous disassembly of the micrometer-sized agglomerates upon stretching of the PAPy chains below the LCST, at least if the PAPy block is long enough. For very short homopolymers (see Fig. S13, ESI†), the phase transition is generally broader and there is a visible hysteresis. Most probably this is due to the comparably large hydrophobic alkyl residue combined with a short hydrophilic polymer block. This pronounced amphiphilicity could favor the formation of agglomerates and demixing of polymer and solvent, thus hampering also the reverse process which can be additionally reinforced by the lower PTT of $PAPy^{3.1}$-$TTC_2$. It is worth mentioning at this point that the ratio between these two species is intensity weighted as obtained by the fit (and displayed here), meaning that it is hardly an exact representation of the actual volumetric and number fractions. Instead, one should keep in mind that the scattering intensity in any light scattering experiment is proportional to $R^6$ (with $R$ being the radius of the scattering particle). For the results in Fig. 2 and for our homopolymer solutions this means that the primarily present species is the well-dissolved unimer. Polymeric aggregates are still present but way less abundant. A ratio of 1 : 10 in Fig. 2 corresponds to at least 99 : 1 in terms of the scattering volume and 99999 : 1 in terms of the total number of scattering centers. Although this means that the smaller of the two species is always dominant, it is of special interest for us to show that LCST phenomena are not always as plain and simple as most literature suggests.

### 2.2 Chain extension of PAPy with styrene *via* PISA

The exemplary temperature studies show that the choice of the CTA itself plays a major role for the stability of the different species in aqueous solution. With this knowledge, first assumptions and predictions can be made for the subsequent emulsion polymerization with styrene. Since the size of the most abundant dissolved species of the pure PAPy homopolymer is below 10 nm and no further surfactant is added, the emulsion will be an *ab initio* emulsion polymerization rather than for instance a mini- or microemulsion.[41,42] There are apart from that some expectable differences in the stabilization of the styrene droplets and the emerging micellar aggregates. As the polymer with the $TTC_1$-endgroup should exhibit the lowest ability to stabilize styrene droplets due to the shortest alkyl chain which is not able to penetrate the styrene phase deeply, the polymers with $TTC_2$ and $TTC_3$-endgroups will certainly fulfill this requirement. This can be already concluded during preparation of the polymerization mixture. Upon addition of the styrene monomer to solutions of the different macromolecular CTAs (macroCTAs) it becomes obvious that the different components of the resulting emulsions are by far more likely to macroscopically separate again if a shorter alkyl chain endgroup is used.

Yet, the emulsion polymerizations with $PAPy^{13.8}$-$TTC_1$ show still short inhibition periods for styrene of approximately 90 minutes and a remarkable degree of control indicated by the absence of dead homopolymer and dispersities below 1.3 (see Fig. S17, ESI†).[43] Polymerization rates of the reactions with a total solids concentration of 10% (w/w) and 15% (w/w) are fast compared to literature block copolymer emulsions with PS as the hydrophobic block – that are usually prepared at more than 70 °C – delivering almost quantitative conversion within less than four hours after the start of the chain extension.[33,44,45] The emulsion at 20% (w/w) solids content shows a slight rate retardation which is mainly attributed to the poor stabilization of the styrene droplets and micelles at higher concentrations of styrene. The SEC traces reveal, though, that the chain end livingness of the homopolymer is seemingly quantitative resulting in a successful chain extension with no residual homopolymer and dispersities well below 1.3 for the end products.

The emulsion polymerizations with the $TTC_2$-polymer ($PAPy^{8.2}$-$TTC_2$) exhibit a significantly longer inhibition period and slightly slower reaction rates (compare Fig. S18–S20, ESI†). Shorter stabilizing blocks additionally increase the inhibition period further, presumably due to worse stabilization of the growing micelles. The inverse trend is observed when the length of hydrophilic macroCTA is increased, which coincidently accelerates the rate of the polymerization. Molecular weight dispersities of the final products range from 1.16 to 1.41, showing the tendency to be lower with a lower degree of polymerization (DP) of PS. It is worth mentioning, that *via* this synthetic pathway diblock copolymers can be prepared in moderate reaction times under sustainable reaction conditions (meaning in this case in water up to quantitative conversion with minimum energy consumption) that reach molecular weights up to 114 kDa. Especially in the case of the normally very slowly propagating styrene this constitutes an alternative route to diblock copolymers suitable for a plethora of applications that is unprecedented considering the reaction temperature of 40 °C.[46,47]

The most remarkable reaction kinetics can be found when using $PAPy^{9.7}$-$TTC_3$ as macroCTA (which does not have the carboxylic acid at the α-terminal end). Initially believed to facilitate the diffusion of the styrene monomer from the bigger monomer droplets into the smaller micelles where the reaction takes place, it not only provided high reaction rates and an inhibition of just about 60 minutes, it furthermore yielded

 

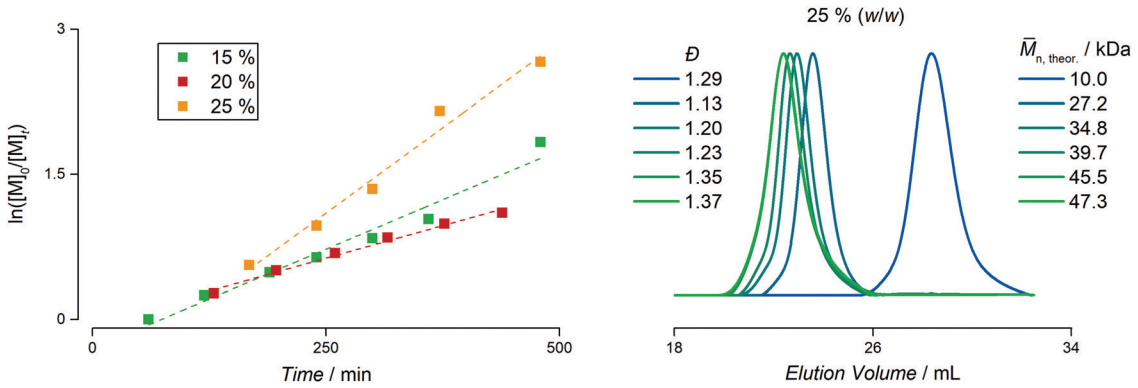


Fig. 3 Left: Pseudo first-order kinetic plot of the styrene emulsion polymerizations with the PAPy$^{9.7}$-TTC$_3$ macroCTA at a total solids concentration of 15% (w/w), 20% (w/w), and 25% (w/w). Right: SEC traces for the samples taken from the kinetic study at 25% (w/w) solids content. The first SEC trace is the macroCTA itself, the remaining traces represent the diblock copolymer samples. The dispersities and overall theoretical molecular weights are given as well.

stable emulsions up to 25% (w/w) solids content (see Fig. 3). The molecular weight distributions become slightly broader with final dispersities between 1.31–1.45, yet no residual homopolymer can be observed in the SEC traces indicating quantitative chain-end fidelity after the first reaction step. Interestingly, the highest reaction rate is found at highest solids content which is exactly the inverse trend compared to the homopolymer with carboxylic acid and butyl endgroups. This again highlights the use of TTC$_3$ as CTA for the emulsion polymerization of styrene. In a nutshell, quantitative conversion can be reached at high solids content yielding diblock copolymers under good control in a PISA formulation without any initiator, surfactant, or other additive. It shows that the concept of light-initiation hence works for highly turbid systems where the penetration depth of the incident light is typically only a small fraction of the overall diameter of the reaction flask.

Up to now we have shown the feasibility of the photoiniferter PISA polymerization to yield PAPy-*b*-PS diblock copolymers up to high solid contents and high molecular weights compared to other CRP methods. Those diblock copolymers constitute very interesting yet easily accessible sources for *e.g.* filtration membrane materials that to date are mainly synthesized *via* an elaborate anionic polymerization procedure.[48–50]

### 2.3 Aqueous dispersions of the PAPy-*b*-PS latexes

It would be regardless, though, to aim for just one purpose with this PISA formulation that almost incidentally yields already pre-formed, submicron-sized organic nanoparticles in an aqueous solution. The herein presented route does not need any initiator or surfactant, so that everything left in the reaction mixture is covalently bound to the nanoparticles. This makes unwanted migration of one of the reaction components in the final product less likely and therefore guarantees improved durability of the products properties.[51–54] Additionally, the hydrophilic stabilizing block yields surface functionality to the nanoparticles without the need of further functionalization steps, which is hardly achievable in a conventional free radical emulsion polymerization.

One of the aims of the herein presented PISA approach is tailoring the size and size distribution of the diblock copolymer aggregates in solution. The three most often observed morphologies of PISA polymers in water are spherical micelles, worm-like micelles, and vesicles (typically increasing in size in that order).[55–57] This work specifically targets the micellar morphology, which has proven to be versatile in its use ranging from biomedical applications[58–60] to coatings[10] or adhesives.[9] This aim is supported by the choice of PS as the hydrophobic core of the micelle due to its high glass transition temperature and hence low ability to undergo reorganization from spherical micelles to worm-like aggregates, especially at the low polymerization temperature of 40 °C.[57,61,62]

Fig. 4 shows exemplary transmission electron microscopy (TEM) images of three diblock copolymers prepared from three different homopolymers with varying endgroups, all with almost quantitative conversion during styrene polymerization. Nomenclature is chosen to be consistent with most other publications on PISA, where subscripts signify the degree of polymerization of the individual block. The superscript at the end stands for the overall theoretical number average molecular weight calculated from the conversion of both blocks and the last part of the name indicates the attached endgroups. Experimental data for the molecular weight (see Tables S2–S4, ESI†) is not meaningful since SEC data need suitable calibration, which is not available for the diblock copolymer.

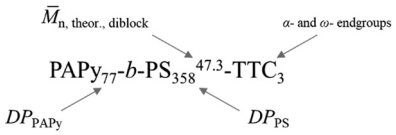


The TEM images in Fig. 4 clearly show that the sizes of the micellar aggregates in aqueous solution are in the same order of magnitude for all the used stabilizing blocks. The radii observed for all TEM measurements are well below 100 nm and by evaluating the size distributions of the latex particles a

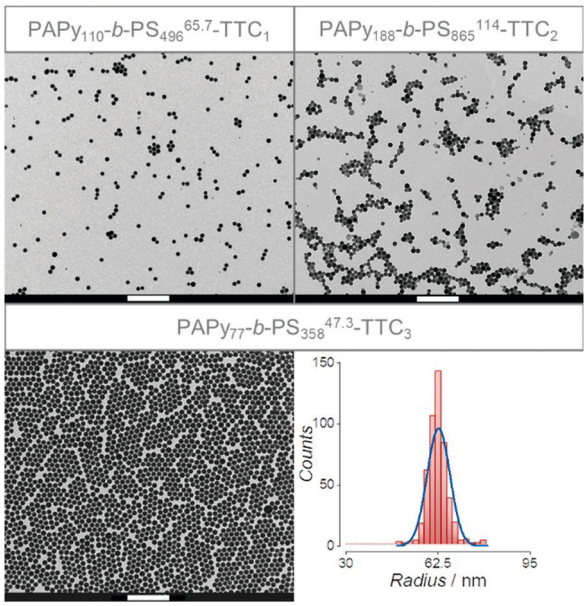


Fig. 4 TEM images of the diblock copolymers prepared from $PAPy^{13.8}$-$TTC_1$ ($PAPy_{110}$-*b*-$PS_{496}^{65.7}$-$TTC_1$, top left), $PAPy^{23.6}$-$TTC_2$ ($PAPy_{188}$-*b*-$PS_{865}^{114}$-$TTC_2$, top right), and $PAPy^{9.7}$-$TTC_3$ ($PAPy_{77}$-*b*-$PS_{358}^{47.3}$-$TTC_3$, bottom left). All scale bars correspond to 1 μm. The size distribution of latex particles taken from analysis of the bottom left image is depicted on the bottom right. A Gaussian fit (blue line) gave a mean radius of 62.7 ± 4.0 nm. For more TEM images and all sized distributions see Fig. S22–S28 (ESI†).

peculiar property becomes evident that fits to the kinetic theory of an *ab initio* emulsion polymerization: size distributions of the resulting micelles are broader if the inhibition period at the beginning of the emulsion polymerization is pronounced, being the case for PISA with PAPy-$TTC_2$ macroCTAs. It is reasonable that this effect can be attributed to a process called secondary nucleation that in our case might be happening at the start of the rate enhancement.[63–65] Due to a better solubilization that is already evident in Fig. 2, light-induced fragmentation of the RAFT endgroup, yielding macromolecular radicals, leads to a desorption of those radicals from the micelles into the aqueous phase. There they can either enter another micelle or add dissolved monomer until the increasing amphiphilicity leads once again to the collapse of the hydrophobic block, forming another micelle. However, further studies need to prove the dependence of size distributions and inhibition periods which is to the best of our knowledge only poorly described in current literature.[66] Nevertheless, it is distinctive that those emulsion polymerizations with the shortest inhibition periods, overcoming nucleation much faster than the remaining growth needs, exhibit the narrowest size distributions (see Fig. 4, bottom right).

To furthermore highlight the potential of the herein presented PISA formulation with $PAPy^{9.7}$-$TTC_3$ to tailor the radius of the resulting spherical micelles while maintaining extraordinarily narrow size dispersities – fairly comparable to those prepared by emulsion polymerizations using surfactants – Fig. 5 depicts the radii of all emulsion polymerizations with this macroCTA measured by TEM as well as the hydrodynamic radii measured by DLS. It is remarkable that the micelles not only linearly increase in size, moreover the size seems to be completely independent of the concentration. In addition to the narrow aggregate size distributions as well as molecular weight distributions this once again emphasizes the potential of this formulation to tailor the properties of PAPy-*b*-PS diblock copolymers.

After examining the size of the particles at room temperature, detailed studies of the solubility behavior have been conducted depending on the temperature. Therefore, dilute samples of the final diblock copolymer micelles were analyzed by DLS in a temperature range from 10–70 °C. Fig. 6 exemplarily shows an evolution of the hydrodynamic radii of $PAPy_{77}$-*b*-$PS_{358}^{47.3}$-$TTC_3$ at 0.02% (w/w) solids concentration.

The DLS data for the diblock copolymers were fitted with the same routine as the homopolymer solutions. For all PISA samples, however, the most probable fit solution as well as CONTIN analysis indicated that the analyzed dispersions only consisted of one particle species in the range of a few ten to one hundred nanometers depending on the DP as already depicted in Fig. 5. This leads to the conclusion that there are no unimers or otherwise dissolved polymer chains left that are not aggregated into micelles. These micelles in turn exhibit an interesting behavior: upon heating of the particle dispersion, the hydrodynamic radius decreases as an almost linear function of the temperature with a slight decline in the shrinking rate towards the end of the heating ramp between 60 °C and 70 °C; a behavior typically observed in microgels.[67,68] It is worth mentioning that the reduction in size is only attributed to the collapse of the corona block. Assuming a fully stretched PAPy chain, this reduction correlates to almost 50% of the overall contour length of this block. The decrease in size is fully reversible until the aggregate size reaches its initial value in the cold state. Most importantly, no coagulates were observable which is in strong contrast to the observations of the PAPy homopolymers. Particle aggregation above the LCST of the homopolymer resulted in a sharp increase of the hydrodynamic

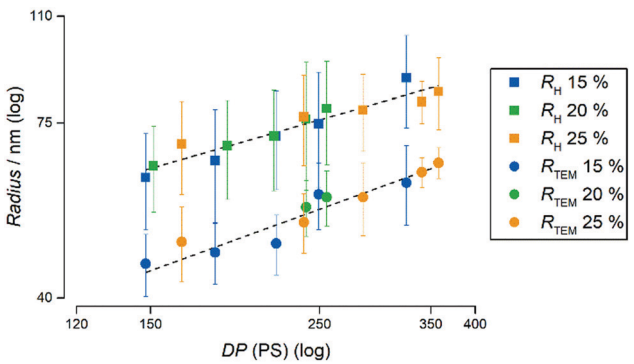


Fig. 5 Evolution of the radii of all polymers made from the $PAPy^{9.7}$-$TTC_3$ macroCTA at 15% (w/w), 20% (w/w), and 25% (w/w) solids concentration compared to the degree of polymerization (DP) of PS. The radii measured by TEM are depicted as circles and the hydrodynamic radii calculated from DLS measurements are depicted as squares. The respective PDI values can be found in Fig. S35 (ESI†).

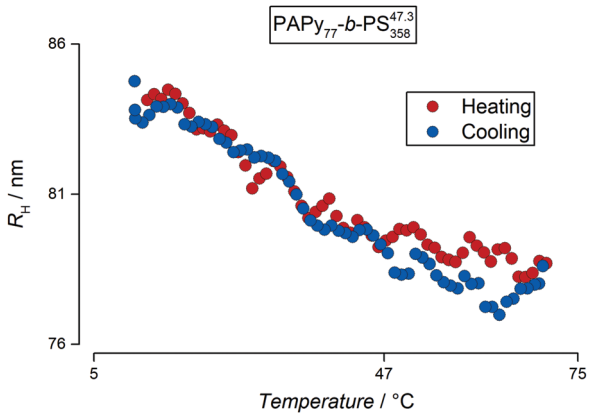


Fig. 6 Evolution of the hydrodynamic radii of $PAPy_{77}$-*b*-$PS_{358}^{47.3}$-$TTC_3$ at 0.02% (w/w) solids concentration with temperature calculated from DLS measurements. The red dots represent the radii during heating of the polymer dispersion and the blue dots represent the respective radii during the cooling step. The most probable fit solution yielded one distribution of particle sizes. The PTT of the used homopolymer is also depicted on the temperature axis.

radius; when the system was given a few hours to equilibrate, these aggregates precipitated from solution.

This does not happen for the diblock copolymer aggregates made by PISA in water. The same observation was made for a more complex system in an earlier work by Eggers *et al.*[33] In contrast to other previous studies for a similar diblock copolymer system prepared by forced self-assembly after the polymerization, the PISA-made micelles stay stabilized in water and tolerate much higher temperatures than the actual phase transition.[69] The lack of agglomeration can be attributed to two major reasons; the first one is the high glass transition temperature ($T_g$) of the PAPy block (142 °C of the dry homopolymer; collapsed PAPy in water might show a lower $T_g$ due to partial hydration)[35] that makes the micelle behave like a solid sphere rather than an aggregate with a dense core and a soft corona which potentially entangles with the corona of adjacent micelles. The second reason could be the comparatively low DPs of the herein used homopolymers which are perhaps below or in the range of the entanglement molecular weight of PAPy. Both reasons – a high $T_g$ and short DPs – attribute to only weak interaction between different micelles and hence inhibit agglomeration. With reasonable certainty we can exclude charge stabilization effects that might arise in the case of $TTC_1$ and $TTC_2$ end-capped polymers due to dissociated carboxylic acids at a solution pH of 5. Since all $TTC_3$ end-capped micelles (that do not carry any charges) are also stable at elevated temperatures, we hypothesize that DP and $T_g$ are the most influential parameters.

However, this can hardly be the reason for the gradual size transition that the micellar aggregates undergo upon heating. A more plausible explanation lies in the free volume of the solubilized corona and the hydrophobicity of the adjacent PS core. Due to densely packed PAPy chains on the surface of the micelle, the water molecules are not able to penetrate the whole corona which lowers the solubility slightly and shifts the onset of the phase transition to lower temperatures. Additionally, these closely packed chains cannot collapse freely and repel the water molecules out of the initially solubilized corona progressively, making the collapse a rather gradual feature compared to the analogous homopolymers (Fig. 7). Given that the thermoresponse is not stepwise but stretched over a wide range of temperatures, yet reversible with no hysteresis, the terminology stipulates the use of 'thermosensitive' instead of 'thermoresponsive'.

The last thing to prove for our PISA system is that the sensitivity is not a onetime feature. Therefore, we conducted a series of DLS measurements where we calculated the hydrodynamic radii during three heating–cooling cycles. The result for an exemplary sample (this time for a diblock copolymer with a $TTC_1$ endgroup) is depicted in Fig. 8. The evolution of the hydrodynamic radii during repeated cycles of heating and cooling indeed shows that the thermosensitivity is a repetitive property. The fact that the minima and maxima of the hydrodynamic radius are reached at similar temperatures while no precipitates have formed during more than 28 hours of heating to 70 °C and cooling to 10 °C furthermore underlines the predictability and durability of the examined latex dispersions.

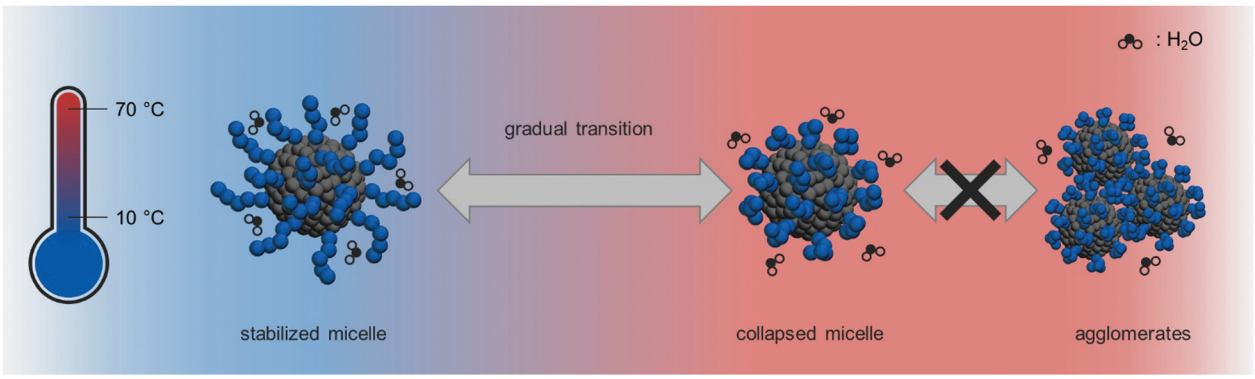


Fig. 7 Molecular scheme of the thermosensitivity of PAPy-*b*-PS spherical micelles prepared *via* PISA. At low temperatures, the hydrophilic corona is solubilized by water. Upon heating, water molecules are repelled from the surface and the PAPy block collapses, but the aggregate is still stabilized. No agglomeration takes place due to unfavorable interaction among different micelles.

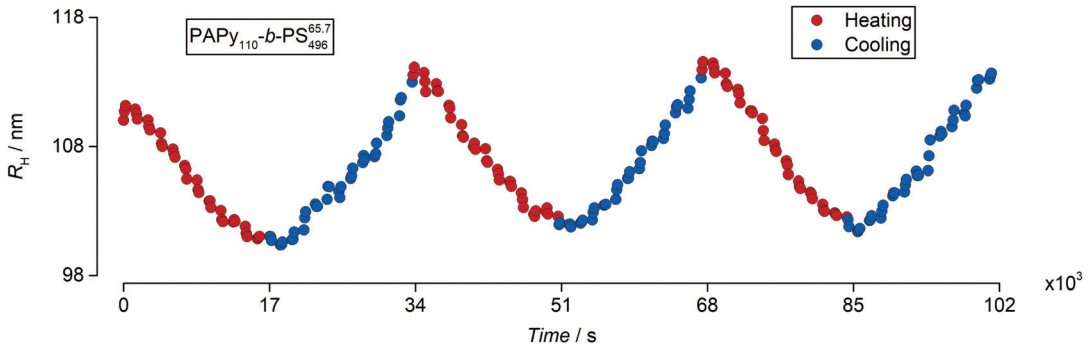


Fig. 8 Evolution of the hydrodynamic radii of $PAPy_{110}$-*b*-$PS_{496}^{65.7}$-$TTC_1$ at 0.02% (w/w) solids concentration with temperature during three heating–cooling cycles calculated from DLS measurements. The red dots represent the radii during heating of the polymer dispersion and the blue dots represent the respective radii during the cooling step. The times marked on the *x*-axis represent the intervals of heating and cooling.

# 3 Conclusion

We presented the photoiniferter two-step solution–emulsion polymerization of PAPy-*b*-PS diblock copolymers with three different endgroups. During the first step, PAPy is formed in a continuous microfluidic process and its peculiar thermo-responsiveness is evaluated depending on the endgroup of the homopolymer. It becomes evident that the aggregation behavior strongly depends on the amphiphilicity and chain length of the used PAPy while endgroups with carboxylic acids additionally promote thermal reorganization. In the second step, we demonstrated the feasibility of the photoiniferter emulsion polymerization of styrene in water at 40 °C yielding fast reaction rates with no inhibition period and reaching quantitative conversion within five to eight hours by using the most suitable endgroup ($TTC_3$). This chain extension constitutes a remarkable example of how conventional emulsion formulations can be replaced by novel methods that work without surface-motile low molecular weight surfactants, volatile organic solvents, and even initiators, paving the way for greener and economically advantageous reactions. The resulting micellar nanoobjects obtained from this PISA approach can be straightforwardly tuned in size by controlling the DP of the PS block. Additionally, TEM images prove that this surfactant-free pathway yields spherical micelles with exceptionally narrow size distributions while the individual polymer chains forming these micelles are also uniform in composition and molecular weight, respectively. The thermo-sensitivity of the diblock copolymer latexes in aqueous solutions was proven to be predictable and remarkably linear over repeated cycles. A typical size decrease of almost 15% was observed upon heating of the dispersion up to 70 °C, with complete reversibility and no formation of precipitates. The PAPy-*b*-PS diblock copolymers prepared *via* the herein presented minimum-ingredient and economical pathway are potential candidates for a plethora of applications like filtration membranes, temperature-sensitive coatings, or adhesives (besides many more) due to the straightforward tunability of the reaction and hence product properties. Molecular weights can be altered from a few ten kDa to more than 100 kDa while the size of the spherical micelles formed by PISA can be coincidently tailored in the range from a few ten nanometers to more than 100 nm. Additionally, long-term tests of the concentrated dispersions prove colloidal stability up to six months after preparation.

# 4 Methods

## 4.1 Materials

Styrene (Sigma Aldrich, 99%) was deinhibited over activated basic alumina prior to each polymerization. The RAFT agents $TTC_2$ (ABCR, 97%) and $TTC_3$ (ABCR, 97%) were used as received. The chemicals used as reactants, acryloyl chloride (ABCR, 96%, stabilized with phenothiazine), pyrrolidine (Acros, 99%), butanethiol (Sigma Aldrich, 99%), potassium hydroxide (Merck, >85%), carbon disulfide (Merck, 99%), *p*-tosyl chloride (Merck, 98%), and 4,4′-azobis(4-cyanopentanoic acid) (Sigma Aldrich, 98%) were used as received. All solvents for reactions, purifications, and NMR, dichloromethane (Acros, 99.9%), 1,4-dioxane (Grüssing, 99%), dimethylformamide (VWR, 99.5%), acetone (Merck, 99%), methyl acetate (Merck, 99%), *n*-hexane (VWR Chemicals, 95%), chloroform-$d_1$ (Euriso-Top, 99.8%), and tetrahydrofuran-$d_8$ (Euriso-Top, 99.5%) were used without further purification. All other chemicals, sodium chloride Grüssing (99%), $KHSO_4$ (Grüssing, 99%), $NaHCO_3$ (Grüssing, 99%), $Mg_2SO_4$ (Grüssing, 99%), and activated basic aluminum oxide (Merck, 99%, grain size between 0.063–0.200 mm) were also used as received.

## 4.2 Synthesis of APy

The synthesis of *N*-acryloylpyrrolidine was adapted from the synthesis of *N*-acryloylpiperidine as described by Jo *et al.*:[70] a solution of acryloyl chloride (7.5 mL, 92 mmol, 1 eq.) in $CH_2Cl_2$ (50 mL) was added dropwise during 30 minutes to a solution of pyrrolidine (15.0 mL, 183 mmol, 2 eq.) in $CH_2Cl_2$ (100 mL) at 0 °C under $N_2$ atmosphere and subsequently stirred for another two hours. During the reaction the flask was permanently flushed with $N_2$ to take away the emerging HCl.

The solution was then washed with brine (100 mL), an aqueous solution of $KHSO_4$ (1 M, 100 mL), brine (100 mL), an aqueous solution of $NaHCO_3$ (5% (w/w), 100 mL), and again brine (100 mL). The organic phase was dried over $Mg_2SO_4$,

 

evaporated to dryness and filtered over activated basic alumina to yield a light-yellow oil (5.84 g, 50.7%).

### 4.3 Synthesis of $TTC_1$

The synthesis of 4-cyano-4-(butylsulfanylthiocarbonyl)sulfanylpentanoic acid was adapted from the synthesis of 4-cyano-4-(propylsulfanylthiocarbonyl)sulfanylpentanoic acid as described by Xu *et al.*:[71] 1-butanethiol (5.00 mL, 467 mmol, 1 eq.) was added dropwise to a solution of potassium hydroxide (3.2834 g, 585 mmol, 1.25 eq.) in water (11.0 mL). After stirring for 30 minutes, carbon disulfide (2.80 mL, 464 mmol, 1 eq.) was added. The mixture was stirred vigorously at room temperature for 1 hour and subsequently cooled to 0 °C. A solution of *p*-tosyl chloride (4.4350 g, 233 mmol, 0.5 eq.) in acetone (22.5 mL) was added dropwise for 20 minutes and stirred for another 2 hours. The excess acetone was removed on a rotary evaporator and the remaining red solution was extracted with dichloromethane (3 × 50 mL). The combined organic phases were washed with water (50 mL), dried over $Mg_2SO_4$ and evaporated to dryness to yield solid bis(butylsulfanylthiocarbonyl)disulfide (12.4623 g, 81%).

A solution of bis(butylsulfanylthiocarbonyl)disulfide (5.0156 g, 152 mmol, 1 eq.) and 4,4′-azobis(4-cyanopentanoic acid) (5.3098 g, 189 mmol, 1.25 eq.) in methyl acetate (65 mL) was heated to reflux for 24 hours. The solution was evaporated to dryness and the product was purified by silica gel column chromatography with methyl acetate : *n*-hexane (1 : 2 (v/v)) as mobile phase to yield 4-cyano-4-(butylsulfanylthiocarbonyl)sulfanylpentanoic acid (5.9142 g, 67%).

### 4.4 PhotoRAFT polymerization of APy

In a typical photoRAFT polymerization of APy, $TTC_2$ (0.0498 g, 0.123 mmol, 1 eq.) and APy (1.4358 g, 11.5 mmol, 93 eq.) were dissolved in a mixture of water (3.37 g) and 1,4-dioxane (5.06 g). Dimethylformamide (0.3 mL) was added as an internal reference for $^1$H-NMR analysis and an initial sample was taken. The solution was connected to the isocratic pump of the millireactor and purged with $N_2$ for 10 minutes at 0 °C. The glass chip millireactor (2 mL, static mixer) was heated to 70 °C and the flowrate was set to 0.1 mL min$^{-1}$ yielding a residence time of 20 minutes. A UV-LED (OmniCure® AC450) with self-made beam-widening (10 × 10 cm) and a thin plexiglass shield to mitigate the intensity to 30 mW cm$^{-2}$ was used as light source 5 cm above the chip surface. A crude $^1$H-NMR sample in chloroform-$d_1$ was taken after the reaction to determine the monomer conversion. The product was precipitated three times in cold *n*-hexane, filtered and dried *in vacuo* overnight.

For the polymerizations with $TTC_1$, the flowrate was set to 0.05 mL min$^{-1}$ to give a residence time of 40 minutes. In the case of $TTC_3$, pure 1,4-dioxane was used as solvent to ensure better solubility of the less hydrophilic CTA.

### 4.5 PhotoRAFT emulsion polymerization of styrene

In a typical photoRAFT emulsion polymerization of styrene in batch, $PAPy^{9.7}$-$TTC_3$ (0.0502 g, 5.02 μmol, 1 eq.) was dissolved in Milli-Q® water (1.0 mL) and styrene (0.2004 g, 1.92 mmol, 383 eq.) was added.‡ The resulting emulsion was homogenized for 30 minutes at 1000 rpm, subsequently purged with $N_2$ for 10 minutes at 0 °C and immersed into an oil bath at 40 °C. The same lamp used for the homopolymerizations was directed at the sample in a distance of 5 cm, the sample was stirred at 600 rpm and the intensity was set to 30 mW cm$^{-2}$. Crude polymer samples were taken from the reaction mixture at different times under $N_2$ protection. These samples were used for $^1$H-NMR analysis in tetrahydrofuran-$d_8$, GPC measurements, and diluted to 0.2% (w/w) for TEM and 0.02% (w/w) for DLS, respectively.

### 4.6 Analytics

**4.6.1 NMR.** $^1$H-NMR-spectra were measured with a Bruker AVANCE™ II 400 MHz Spectrometer at a temperature of 300 K with 16 scans and a delay of one second for standard spectra and 64 scans and a delay of three seconds for polymer samples. Chloroform-$d_1$ was used as solvent for the homopolymers and the $CHCl_3$-signal used as reference. In case of the diblock copolymers, tetrahydrofuran-$d_8$ was used as solvent and the tetrahydrofuran signal was used as reference. The concentrations were around 10 mg mL$^{-1}$ for all samples. Analysis was realized with the program MestReNova 10.0.

**4.6.2 SEC.** The SEC measurements have been performed at 50 °C when using DMAc as solvent. PS and PMMA were used as reference and the UV-detector was operated at a wavelength of 260 nm. Concentrations of the polymer solutions ranged from 1 mg mL$^{-1}$ to 3 mg mL$^{-1}$. They were measured at a flow rate of 1 mL min$^{-1}$ using an isocratic PSS® SECcurity pump and methyl benzoate (10 μL per 100 mL DMAc) as internal standard. LiCl (0.1 M) was added to the solvent to screen charge interactions between the analyte and the column material. PSS® SDV combination high columns (three columns á 8 × 300 mm) with pore sizes of $10^3$ Å, $10^5$ Å, and $10^6$ Å were used. The detector was a PSS® SECcurity Differential-Refractometer-Detector operated at 50 °C and analysis was made with the software WinGPC UniChrom V8.10.

**4.6.3 UV-VIS.** UV-Vis-spectra were recorded with a PerkinElmer® Lambda 25. Transmission through samples ($c$ = $10^{-5}$–$10^{-3}$ mol L$^{-1}$) was measured from 200–500 nm with a speed of 480 nm min$^{-1}$ at 300 K. A tungsten-halogen lamp (300–3000 nm) and a deuterium lamp (200–400 nm) served as light sources.

**4.6.4 TEM.** TEM images were taken with an Eagle™ 4k HS 200 kV camera on a FEI™ Tecnai™ G2 Spirit TWIN instrument in bright field mode, operating at an accelerating voltage of 120 kV. Images were processed with TEM Imaging & Analysis Offline 4.7 SP3 (FEI™) software and ImageJ 1.51p. Samples were prepared on carbon coated copper grids. Polymer dispersions ($c$ = 2 mg mL$^{-1}$) were dropcast onto the TEM grid before excess of solution was blotted with filter paper.

**4.6.5 Visual turbidimetry.** For the first estimation of the cloud points of PAPy homopolymers, visual turbidimetry was used. The polymer was dissolved in Milli-Q® water at a

‡ For the use of $TTC_1$ and $TTC_2$ endgroups the solution pH was in all cases around 5 while for $TTC_3$ the solution pH remained at 7.

concentration of 10 mg $mL^{-1}$ and stirred for at least 2 hours. The cloud points were then determined in three heating–cooling cycles with a temperature accuracy of 0.1 °C – as measured with a Voltcraft® PL-120-T1 thermometer directly in the solution – and a reproducibility of $<0.3$ °C deviation. The cloud point was therefore defined as the onset of the clouding. For the heating step, the solution was immersed into a water bath with a heating rate of approximately 1 °C $min^{-1}$. The cooling was performed at room temperature.

**4.6.6 DLS.** The DLS measurements were conducted on two different setups. Both systems based on an ALV®/CGS-3 Compact Goniometer-System either using an ALV®/LSE-5003 Multiple Tau Digital Correlator (V.1.5.6.) in combination with a JDS Uniphase® 1145/P laser (He–Ne, 632.8 nm, 22.5 mW) or an ALV®/LSE-5004 Multiple Tau Digital Correlator (V.1.7.9.) in combination with a Cobolt™ Samba™ 50 laser (Nd:YAG, 532 nm, 400 mW) and the ALV® Digital Correlator Software 3.0. The measuring angle was set to 90° for all measurements and every individual measurement was conducted for 60 s. The sample vials consisted of quartz glass and were placed into a measurement cell filled with toluene. The temperature-dependent viscosity and refractive index of the solvents were automatically corrected according to tabulated values. The toluene bath and thus the samples were tempered by a Julabo® F25 thermostat working with a mixture of water and ethylene glycol and delivering a temperature accuracy of 0.01 °C.

Temperature-dependent DLS measurements of the homopolymers were conducted in temperature steps of 1 °C with three measurements per temperature. The polymer solutions were prepared 24 hours prior to the measurements at a concentration of 10 mg $mL^{-1}$ by dissolving the polymer in Milli-Q® water that was pre-filtered through microporous regenerated cellulose filters (average pore diameter: 200 nm). The maximum temperature was chosen to be approximately 3 °C above the cloud point estimated by visual turbidimetry.

Temperature-dependent DLS measurements of the diblock copolymer aggregates were conducted in temperature steps of 5 °C with three measurements per temperature. The polymer emulsions were withdrawn directly from the polymerization mixture and diluted with pre-filtered Milli-Q® water to 0.2 mg $mL^{-1}$ to avoid multiple scattering. The temperature range was set to 10–70 °C (unless stated otherwise). For standard measurements at room temperature, the same concentrations were used as for the temperature-dependent measurements. Analysis of all DLS measurements was conducted with a self-written program based on a cumulant approach up to the third order cumulant. For specific samples an additional CONTIN analysis was made.

## Author contributions

F. L. contributed to the experimental setup, data acquisition and interpretation, analysis as well as validation, and the writing of the manuscript. V. A. was responsible for funding acquisition, project administration, as well as interpretation of the experimental data and writing of the manuscript.

## Conflicts of interest

There are no conflicts to declare.

## Acknowledgements

F. L. and V. A. would like to thank Dr Birgit Fischer for prolific discussions about the analysis of DLS data. F. L. furthermore acknowledges the work of Katharina Nieswandt, Vanessa Meyen, and Sascha B. Lemich on preceding studies regarding the present polymer system.

## References

1 W. D. Harkins, *J. Am. Chem. Soc.*, 1947, **69**, 1428–1444.
2 W. D. Harkins, *J. Polym. Sci.*, 1950, **5**, 217–251.
3 R. W. Lines and B. V. Miller, *Powder Technol.*, 1979, **24**, 91–96.
4 E. Gombocz, D. Tietz, S. S. Hurtt and A. Chrambach, *Electrophoresis*, 1987, **8**, 261–271.
5 R. T. Fisk, *US Pat.*, US3088875A, 1959.
6 S. Kasempimolporn, N. Chaiyabutr and V. Sitprija, *Current Laboratory Techniques in Rabies Diagnosis, Research and Prevention*, Academic Press, 2014, pp. 141–145.
7 E. D. Korn and R. A. Weisman, *J. Cell Biol.*, 1967, **34**, 219–227.
8 M. Monzon, M. Lock and J. Galloway, EP0364629A1, 1988.
9 J. Dejeu, M. Bechelany, L. Philippe, P. Rougeot, J. Michler and M. Gauthier, *ACS Appl. Mater. Interfaces*, 2010, **2**, 1630–1636.
10 Y. Li, R. Liu, J. Wang and X. Tang, *Prog. Org. Coat.*, 1992, **21**, 101–107.
11 S. W. Prescott, M. J. Ballard, E. Rizzardo and R. G. Gilbert, *Macromolecules*, 2002, **35**, 5417–5425.
12 C. J. Ferguson, R. J. Hughes, B. T. T. Pham, B. S. Hawkett, R. G. Gilbert, A. K. Serelis and C. H. Such, *Macromolecules*, 2002, **35**, 9243–9245.
13 C. J. Ferguson, R. J. Hughes, D. Nguyen, B. T. T. Pham, R. G. Gilbert, A. K. Serelis, C. H. Such and B. S. Hawkett, *Macromolecules*, 2005, **38**, 2191–2204.
14 M. Semsarilar and S. Perrier, *Nat. Chem.*, 2010, **2**, 811.
15 M. F. Cunningham, J. D. Campbell, Z. Fu, J. Bohling, J. G. Leroux, W. Mabee and T. Robert, *Green Chem.*, 2019, **21**, 4919–4926.
16 J. Ho, B. Mudraboyina, C. Spence-Elder, R. Resendes, M. F. Cunningham and P. G. Jessop, *Green Chem.*, 2018, **20**, 1899–1905.
17 J. Wang and K. Matyjaszewski, *Macromolecules*, 1995, **28**, 7572–7573.
18 K. Matyjaszewski and J. Xia, *Chem. Rev.*, 2001, **101**, 2921–2990.

 

19 P. G. Griffiths, E. Rizzardo and D. H. Solomon, *Tetrahedron Lett.*, 1982, **23**, 1309–1312.
20 T. P. Le, G. Moad, E. Rizzardo and S. H. Thang, WO1998001478A1, 1997.
21 J. Chiefari, Y. K. Chong, F. Ercole, J. Krstina, J. Jeffery, T. P. T. Le, R. T. A. Mayadunne, G. F. Meijs, C. L. Moad and G. Moad, *Macromolecules*, 1998, **31**, 5559–5562.
22 B. P. Fors and C. J. Hawker, *Angew. Chem., Int. Ed.*, 2012, **51**, 8850–8853.
23 Y. Guillaneuf, D. Bertin, D. Gigmes, D.-L. Versace, J. Lalevée and J.-P. Fouassier, *Macromolecules*, 2010, **43**, 2204–2212.
24 T. Otsu and M. Yoshida, *Die Makromol. Chemie, Rapid. Commun.*, 1982, **3**, 127–132.
25 T. G. McKenzie, E. Colombo, Q. Fu, M. Ashokkumar and G. G. Qiao, *Angew. Chem., Int. Ed.*, 2017, **56**, 12302–12306.
26 M. Kamigaito, T. Ando and M. Sawamoto, *Metal-catalyzed living radical polymerization*, 2001, vol. 101.
27 A. Reyhani, T. G. McKenzie, H. Ranji-Burachaloo, Q. Fu and G. G. Qiao, *Chem. – Eur. J.*, 2017, **23**, 7221–7226.
28 R. Chapman, A. J. Gormley, K.-L. Herpoldt and M. M. Stevens, *Macromolecules*, 2014, **47**, 8541–8547.
29 S. Kumagai, K. Nagai, K. Satoh and M. Kamigaito, *Macromolecules*, 2010, **43**, 7523–7531.
30 Y. Wang, M. Fantin, S. Park, E. Gottlieb, L. Fu and K. Matyjaszewski, *Macromolecules*, 2017, **50**, 7872–7879.
31 S. Perrier, *Macromolecules*, 2017, **50**, 7433–7447.
32 C. N. Urbani and M. J. Monteiro, *Macromolecules*, 2009, **42**, 3884–3886.
33 S. Eggers and V. Abetz, *Polymers*, 2017, **9**, 668–691.
34 N. Lucht, S. Eggers and V. Abetz, *Polym. Chem.*, 2017, **8**, 1196–1205.
35 S. Eggers, T. Eckert and V. Abetz, *J. Polym. Sci., Part A: Polym. Chem.*, 2018, **56**, 399–411.
36 M. Wang, S. Harrisson, M. Destarac and J.-D. Marty, *J. Supercrit. Fluids*, 2019, **152**, 104572.
37 J.-F. Lutz, Ö. Akdemir and A. Hoth, *J. Am. Chem. Soc.*, 2006, **128**, 13046–13047.
38 D. Fournier, R. Hoogenboom, H. M. L. Thijs, R. M. Paulus and U. S. Schubert, *Macromolecules*, 2007, **40**, 915–920.
39 Y. Zhang, S. Furyk, L. B. Sagle, Y. Cho, D. E. Bergbreiter and P. S. Cremer, *J. Phys. Chem. C*, 2007, **111**, 8916–8924.
40 S. Eggers, B. Fischer and V. Abetz, *Macromol. Chem. Phys.*, 2016, **217**, 735–747.
41 R. G. Gilbert, *Emulsion polymerization: a mechanistic approach*, Academic Press, London, 1995.
42 A. van Herk, *Chemistry and Technology of Emulsion Polymerisation*, 2007.
43 M. Semsarilar, E. R. Jones and S. P. Armes, *Polym. Chem.*, 2014, **5**, 195–203.
44 T. Boursier, I. Chaduc, J. Rieger, F. D'Agosto, M. Lansalot and B. Charleux, *Polym. Chem.*, 2011, **2**, 355–362.
45 Y. Luo, X. Wang, B. G. Li and S. Zhu, *Macromolecules*, 2011, **44**, 221–229.
46 F. Lauterbach, M. Rubens, V. Abetz and T. Junkers, *Angew. Chem., Int. Ed.*, 2018, **57**, 14260–14264.
47 K. Jung, J. Xu, P. B. Zetterlund and C. Boyer, *ACS Macro Lett.*, 2015, **4**, 1139–1143.
48 A. Jung, S. Rangou, C. Abetz, V. Filiz and V. Abetz, *Macromol. Mater. Eng.*, 2012, **297**, 790–798.
49 R. A. Mulvenna, J. L. Weidman, B. Jing, J. A. Pople, Y. Zhu, B. W. Boudouris and W. A. Phillip, *J. Membr. Sci.*, 2014, **470**, 246–256.
50 V. Abetz, *Macromol. Rapid Commun.*, 2015, **36**, 10–22.
51 A.-C. Hellgren, P. Weissenborn and K. Holmberg, *Prog. Org. Coat.*, 1999, **35**, 79–87.
52 M. J. Monteiro, M. Sjöberg, J. van der Vlist and C. M. Göttgens, *J. Polym. Sci., Part A: Polym. Chem.*, 2000, **38**, 4206–4217.
53 J. I. Amalvy, M. J. Unzué, H. A. S. Schoonbrood and J. M. Asua, *J. Polym. Sci., Part A: Polym. Chem.*, 2002, **40**, 2994–3000.
54 N. Shirakbari, M. Ebrahimi, H. Salehi-Mobarakeh and M. Khorasani, *J. Macromol. Sci., Part B: Phys.*, 2014, **53**, 1286–1292.
55 B. Karagoz, L. Esser, H. T. Duong, J. S. Basuki, C. Boyer and T. P. Davis, *Polym. Chem.*, 2014, **5**, 350–355.
56 B. Charleux, G. Delaittre, J. Rieger and F. D'Agosto, *Macromolecules*, 2012, **45**, 6753–6765.
57 S. L. Canning, G. N. Smith and S. P. Armes, *Macromolecules*, 2016, **49**, 1985–2001.
58 H. Vihola, A.-K. Marttila, J. S. Pakkanen, M. Andersson, A. Laukkanen, A. M. Kaukonen, H. Tenhu and J. Hirvonen, *Int. J. Pharm.*, 2007, **343**, 238–246.
59 L. M. Johnson, Z. Li, A. J. LaBelle, F. S. Bates, T. P. Lodge and M. A. Hillmyer, *Macromolecules*, 2017, **50**, 1102–1112.
60 L. Esser, N. P. Truong, B. Karagoz, B. A. Moffat, C. Boyer, J. F. Quinn, M. R. Whittaker and T. P. Davis, *Polym. Chem.*, 2016, **7**, 7325–7337.
61 J. Lesage de la Haye, X. Zhang, I. Chaduc, F. Brunel, M. Lansalot and F. D'Agosto, *Angew. Chem., Int. Ed.*, 2016, **55**, 3739–3743.
62 N. P. Truong, M. V. Dussert, M. R. Whittaker, J. F. Quinn and T. P. Davis, *Polym. Chem.*, 2015, **6**, 3865–3874.
63 S. M. Lepizzera and A. E. Hamielec, *Macromol. Chem. Phys.*, 1994, **195**, 3103–3115.
64 B. R. Morrison and R. G. Gilbert, *Macromol. Symp.*, 1995, **92**, 13–30.
65 E. M. Coen, R. G. Gilbert, B. R. Morrison, H. Leube and S. Peach, *Polymer*, 1998, **39**, 7099–7112.
66 P. B. Zetterlund, S. C. Thickett, S. Perrier, E. Bourgeat-Lami and M. Lansalot, *Chem. Rev.*, 2015, **115**, 9745–9800.
67 A. Pich, A. Tessier, V. Boyko, Y. Lu and H.-J. P. Adler, *Macromolecules*, 2006, **39**, 7701–7707.
68 A. Pich, S. Bhattacharya, Y. Lu, V. Boyko and H.-J. P. Adler, *Langmuir*, 2004, **20**, 10706–10711.
69 S. Eggers, F. Lauterbach and V. Abetz, *Polymer*, 2016, **107**, 357–367.
70 Y. S. Jo, A. J. van der Vlies, J. Gantz, S. Antonijevic, D. Demurtas, D. Velluto and J. A. Hubbell, *Macromolecules*, 2008, **41**, 1140–1150.
71 X. Xu, A. E. Smith, S. E. Kirkland and C. L. McCormick, *Macromolecules*, 2008, **41**, 8429–8435.